Table of Contents for the Supplemental materials

Supplementary Figure 1

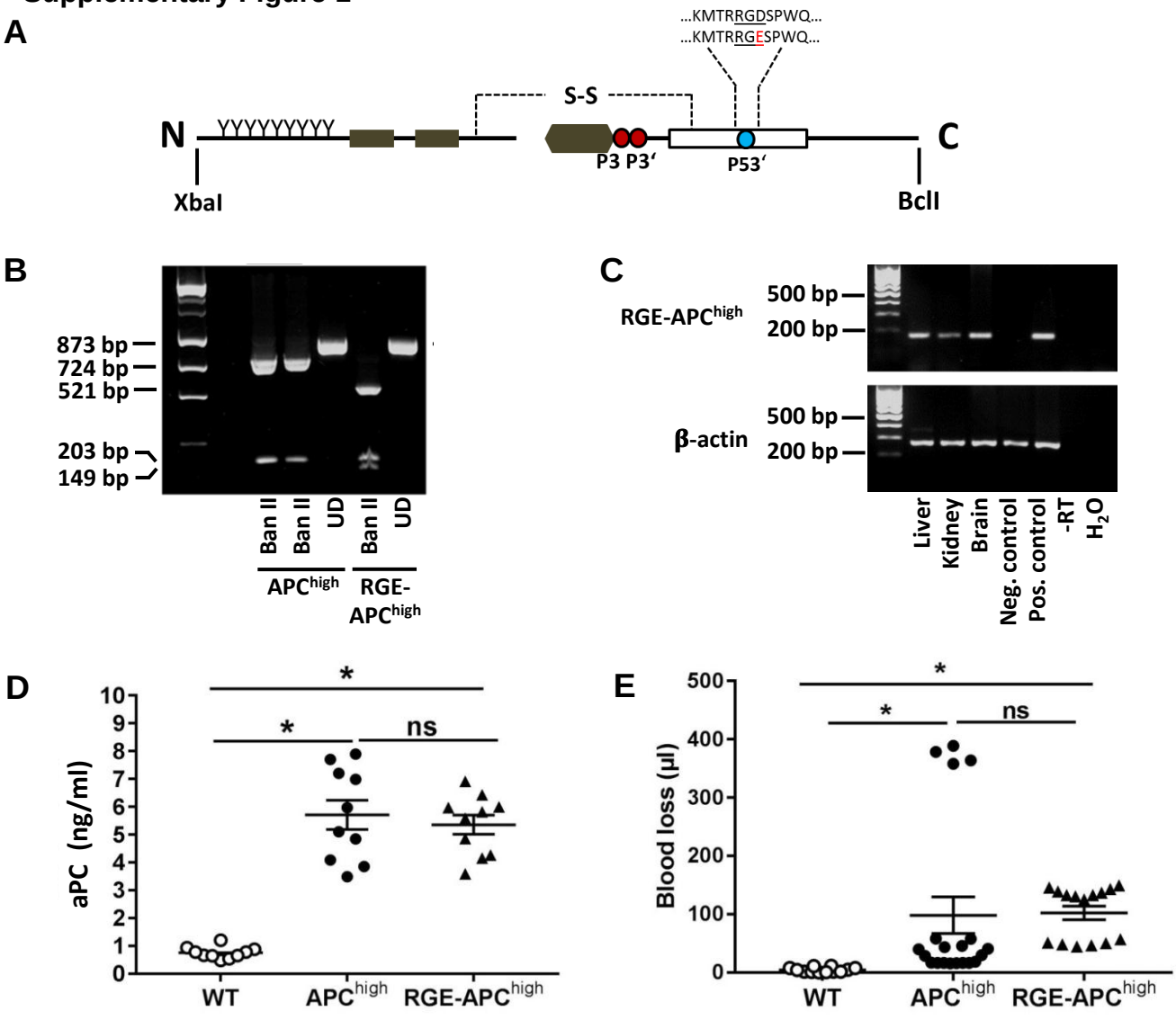

Supplemental Figure 1: Generation and characterization of RGE-APC^{high} mice

(**A**) Scheme of the RGE-APC^{high} transgene. The sequence coding for the RGD sequence was mutated to code for a mutated protein containing RGE (P53′: D222E). As a template, a plasmid coding the hyperactivatable human protein C (PC) mutant (P3: D167F; P3′: D172K, aPC^{high}) was used[10]. "Y" indicates Gla residues, gray rectangular boxes indicate EGF-like domains, the gray hexagon indicates the activation peptide, and the white rectangle indicates the serine protease module. S-S indicates a disulfide bond between the heavy and light chains of PC. The XbaI–Bcl1 fragment was used for subcloning[10].

(**B**) Representative gel images of undigested (UD) and BanII-digested (BanII) amplimers in aPC^{high} and RGE-aPC^{high} mice. The additional BanII restriction site in the RGE-aPC^{high} transgene results in three (149 pb, 203 bp, and 521 bp) instead of two (149 bp and 724 bp, as seen in aPC^{high} mice) fragments upon digestion of an 873 bp PCR amplimer.

(**C**) Representative gel images showing the mRNA expression of the RGE-aPC^{high} transgene in different organs as detected by semiquantitative RT-PCR.

(**D**) Average plasma level of the mutant PC in transgenic APC^{high} and RGE-APC^{high} mice, as determined by activated protein C (aPC) capture assay.

(**E**) Blood loss in mice after a standardized tail cut. Blood loss is increased to a comparable extent both in aPC^{high} and RGE-aPC^{high} mice compared to wild-type mice.

The data shown in dot plots represent the mean ± standard error of the mean (SEM) of at least 10 mice per group; *P<0.05, ns: non significant; D, E: ANOVA with Tukey-adjusted post hoc comparison.

Supplementary Figure 2

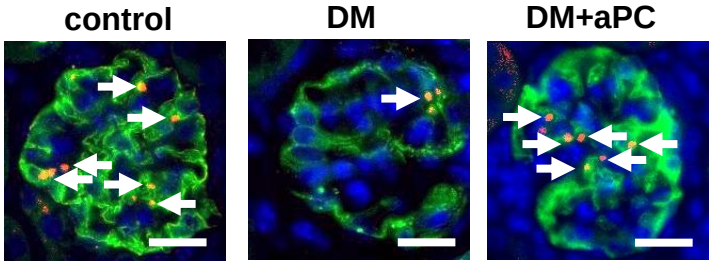

Supplemental Figure 1. Protein C / aPC is glomerularily filtered. Experimental evidence, that protein C / aPC is glomerularily filtered and interacts with β_3 integrin on podocytes.
Representative images showing PC and integrin β_3 interaction in glomeruli (detected by proximity ligation assay, PLA, red) in combination with immunofluorescent staining for nephrin (green) in non-diabetic (control, left), diabetic (DM, middle), and aPC-treated diabetic (DM+aPC, right) mice (age: 24 weeks); representative images, scale bar 20 µm.

Supplementary Figure 3

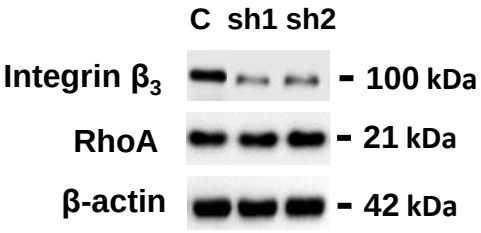

Supplemental Figure 3: Characterizing knockdown of integrin-β_3 in podocytes. Representative immunoblot images showing efficient knockdown of integrin-β_3 (100 kDa) in human podocytes using two disjunct shRNA constructs (shRNA1 and shRNA2, labelled as sh1 and sh2) and a nonspecific shRNA-control (control, C). Expression of RhoA (21 kDa, middle) is not affected. Immunoblot of β-actin (42 kDa, bottom) is shown as loading control.

Supplementary Figure 4

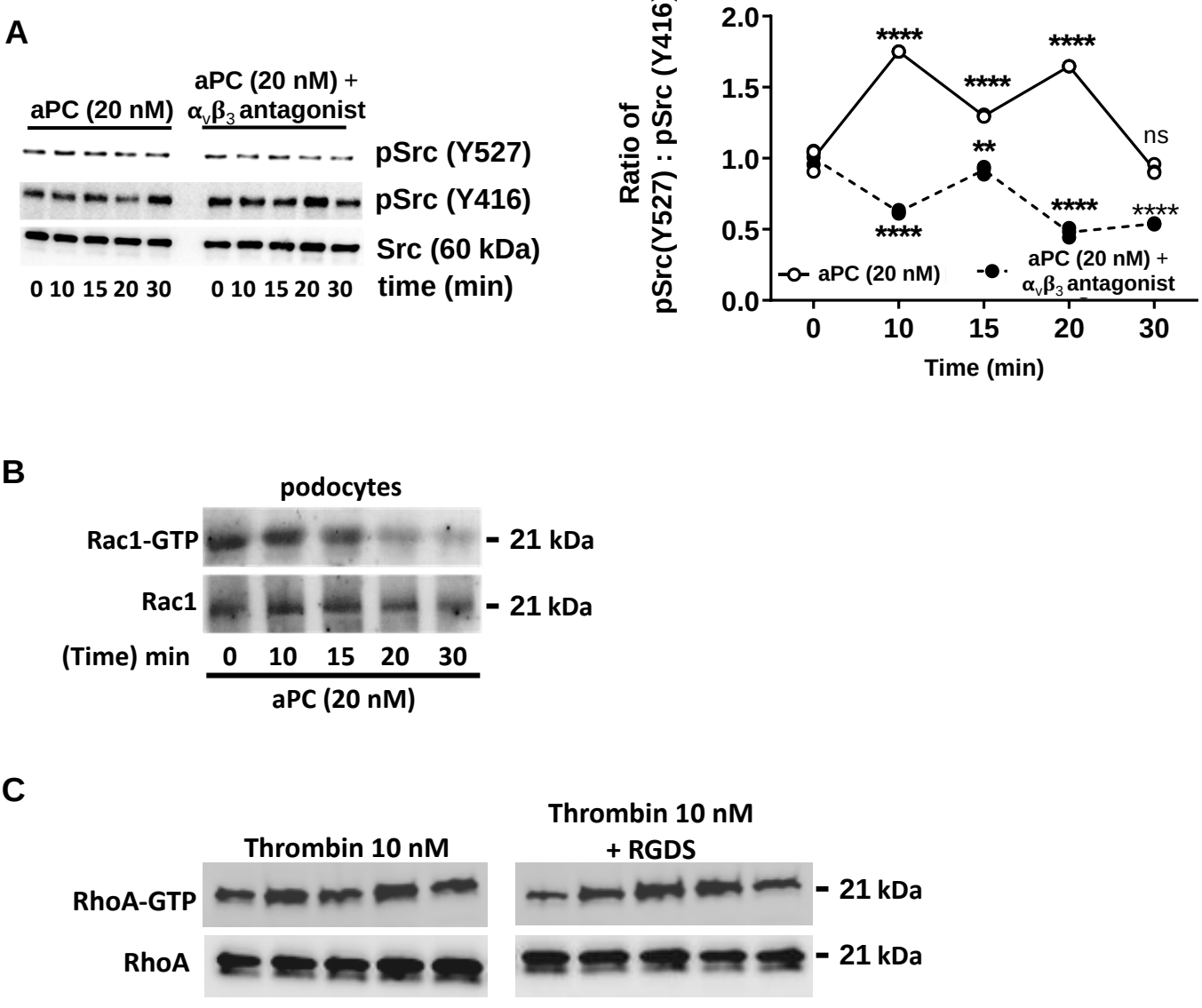

Supplemental Figure 2. aPC-induced signaling in podocytes.

(**A**) Representative immunoblot images showing time-dependent phosphorylation of Src (Y527) and of Src (Y416) upon exposure of human podocytes to aPC alone or aPC plus CycloRGDfv ($\alpha_v\beta_3$ antagonist, left) and dot-blot summarizing data from three independent repeat experiments (right, mean ± SEM of 3); **P<0.01, ****P<0.001; ANOVA with Tukey-adjusted post hoc comparison of stimulated cells to base-line (0 min).

(**B**) Representative immunoblot images showing levels of Rac1-GTP and total Rac1 in podocytes at different timepoints before (0 min) or after stimulation with 20 nM aPC.

(**C**) Representative immunoblot images showing levels of RhoA-GTP and total RhoA in podocytes at different timepoints before (0 min) or after stimulation with 10 nM thrombin alone or 10 nM thrombin plus RGDS (50 µg/ml).

Supplementary Figure 5

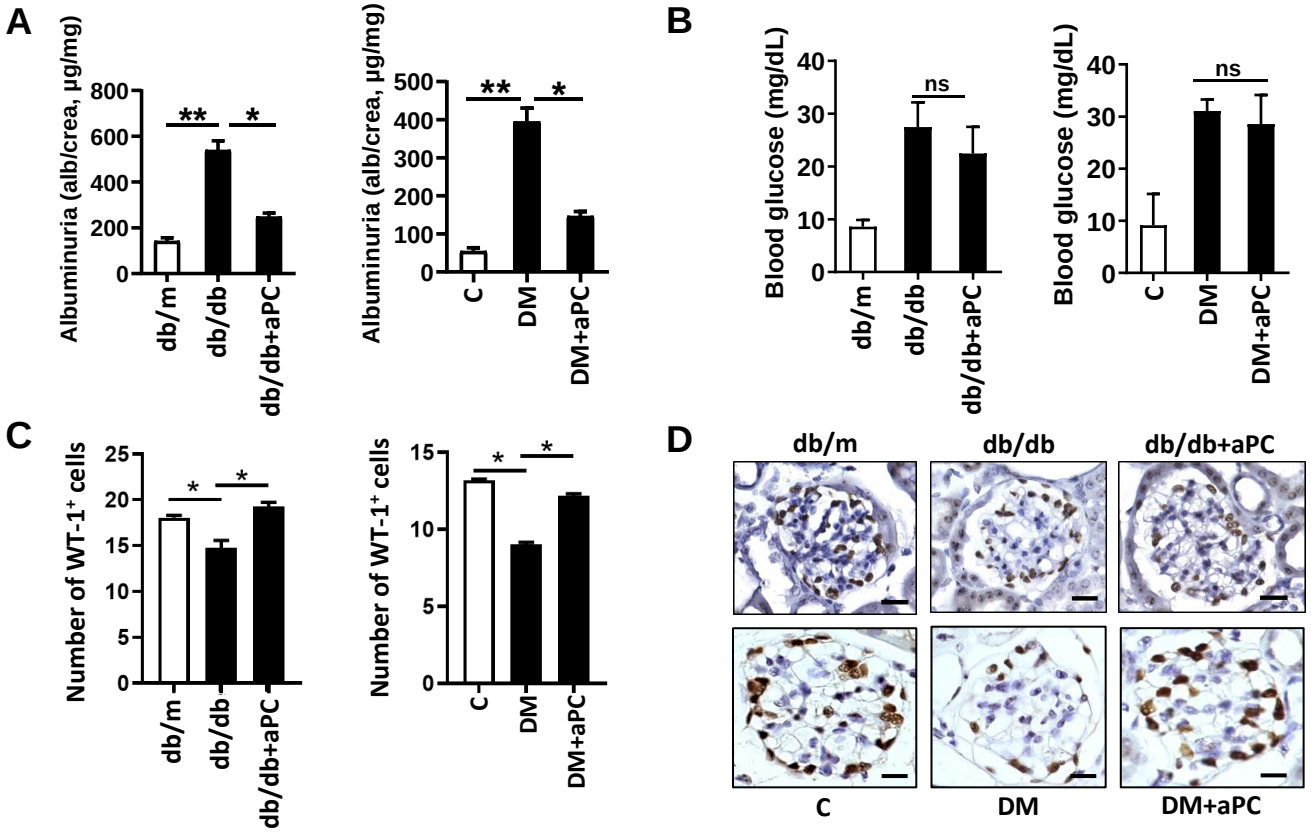

Supplemental Figure 4 Characteristics of experimental mice, corresponding to Figure 4A

Bar graphs summarizing albuminuria (A), blood glucose levels (B), and WT-1 positive glomerular cells (C, exemplary images in D) in non-diabetic control (db/m, C) and diabetic mice without (db/db, DM) or with (db/db+aPC, DM+aPC) aPC treatment. D: Exemplary immunohistochemical images, WT-1 positive cells detected by HRP-DAB reaction, brown; hematoxylin nuclear counterstain, blue, size bar 10 µm.

The bar graphs show the mean ± standard error of the mean (SEM) of at least 5 mice per group; *P<0.05, **P<0.01, ns: non significant; ANOVA with Tukey-adjusted post hoc comparison; diabetic mice were compared do non-diabetic mice, and diabetic mice without were compared to diabetic mice with aPC treatment.

Supplementary Figure 6

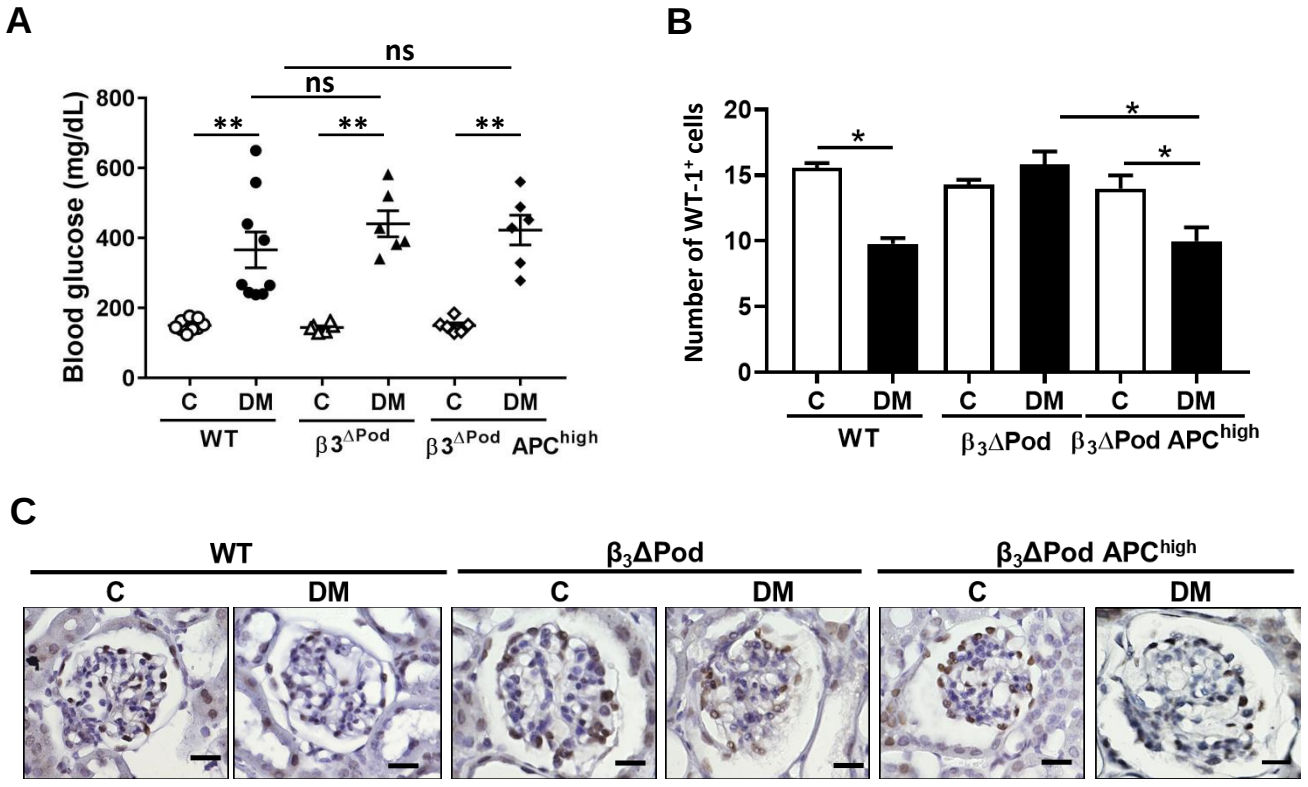

Supplemental Figure 5: Characteristics of experimental mice, corresponding to Figure 4B-G
Dot plot summarizing blood glucose levels (A) and bar graph summarizing WT-1 positive glomerular cells (B, exemplary images in C) in wild-type, $\beta_3\Delta$Pod and $\beta_3\Delta$Pod APC^{high} mice without (control, C) or with (DM) persistent hyperglycemia. C: Exemplary immunohistochemical images, WT-1 positive cells detected by HRP-DAB reaction, brown; hematoxylin nuclear counterstain, blue, size bar 10 µm.
The dot plots and bar graphs show the mean ± standard error of the mean (SEM) of at least 5 mice per group; **P<0.01, ***P<0.001, ns: non significant; ANOVA with Tukey-adjusted post hoc comparison; for each genotype diabetic mice were compared do non-diabetic mice, and diabetic mutant mice were compared to diabetic wild-type mice.

Supplementary Figure 7

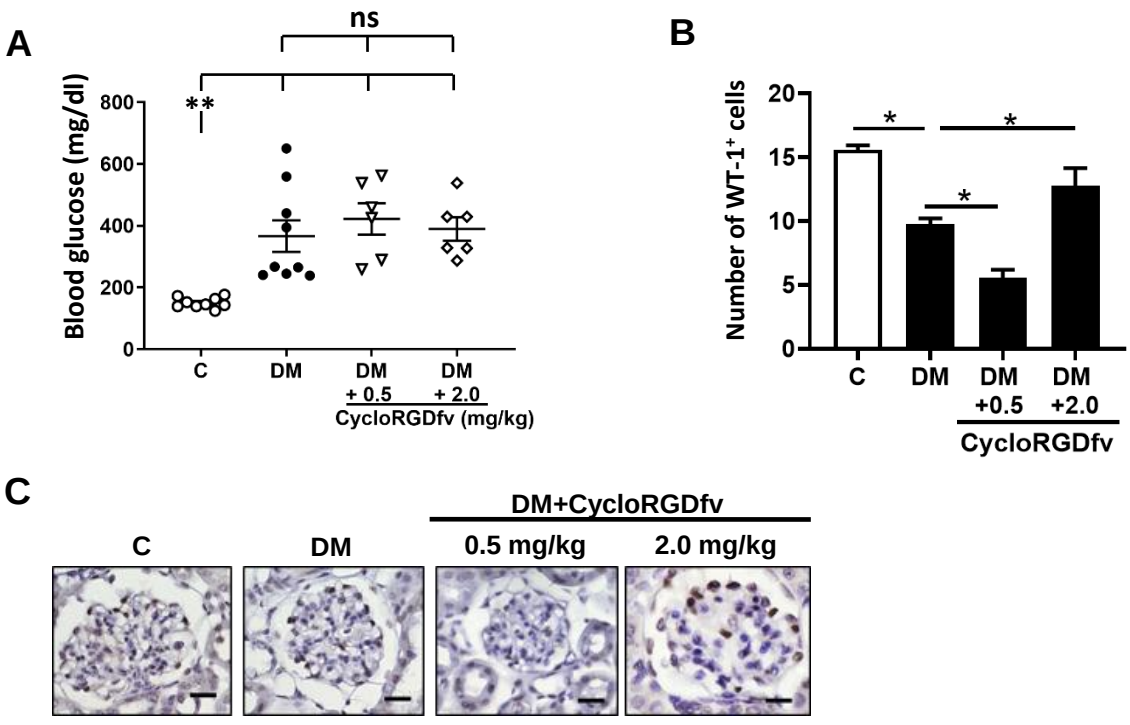

Supplemental Figure 6: Characterization of experimental mice, corresponding to Figure 5

Blood glucose levels (A) and WT-1 positive glomerular cells (B,C) in wild-type mice without (control, C) or diabetic mice injected either with PBS (diabetic control, DM) or with the integrin-$\alpha_v\beta3$ antagonist CycloRGDfv at a low (0.5 mg/kg, DM+0.5) or high (2 mg/kg, DM+2.0) dose. Blood glucose levels do not significantly differ among the diabetic groups (A, dot plot summarizing the results). Compared to control diabetic mice, the frequency of WT-1 positive cells is reduced in diabetic wild-type mice treated with low dose CycloRGDfv, but increased in diabetic wild-type mice treated with high dose CycloRGDfv (B: dot blot summarizing results; C: exemplary images; WT-1: HRP-DAB reaction, brown; hematoxylin nuclear counterstain).

The dot plots and bar graphs show the mean ± standard error of the mean (SEM) of at least 5 mice per group; *P<0.05, **P<0.01, ns: non significant; ANOVA with Tukey-adjusted post hoc comparison; A: diabetic mice were compared do non-diabetic mice, and diabetic mice treated with CycloRGDfv were compared to diabetic control mice; B: diabetic mice without CycloRGDfv were compared to non-diabetic mice, and diabetic mice treated with Cyclo-RGDfv were compared to diabetic control mice.

Supplementary Figure 8

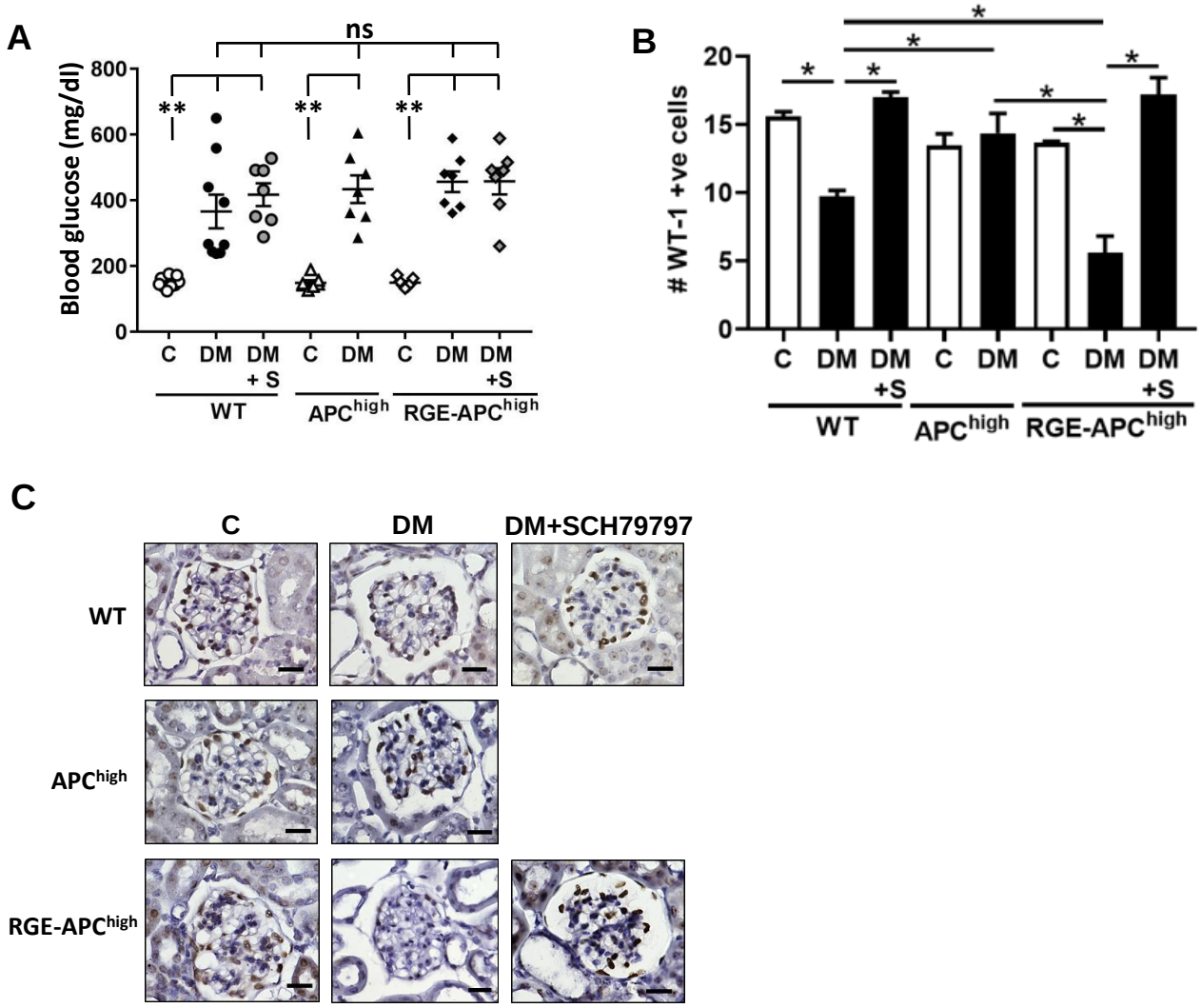

Supplemental Figure 8. Characterization of experimental mice, corresponding to Figure 6

Dot plot summarizing the blood glucose levels (A) and bar graph summarizing WT-1 positive glomerular cells (B) in wild-type, APC^{high}, and RGE-APC^{high} mice without (C) or with (DM) persistent hyperglycemia. Subgroups of diabetic mice were injected with the protease-activated receptor 1 (PAR1) antagonist SHC79797 (DM+S). Blood glucose levels do not significantly differ among the diabetic groups. The frequency of WT-1 positive cells is reduced in diabetic wild-type mice and to a larger extend in RGE-APC^{high} mice. SHC79797 intervention protects from podocyte loss in diabetic mice; C: exemplary images; WT-1: HRP-DAB reaction, brown; hematoxylin nuclear counterstain.

The dot plots and bar graphs show the mean ± standard error of the mean (SEM) of at least 5 mice per group; *P<0.05, **P<0.01; ANOVA with Tukey-adjusted post hoc comparison; for each genotype diabetic mice were compared do non-diabetic mice, diabetic mutant mice were compared to diabetic wild-type mice (without SHC79797 treatment), and diabetic mice treated with SCH79797 were compared to untreated diabetic mice of the same genotype.